DOI: https://doi.org/10.2138/am-2022-8911. http://www.minsocam.org/

A Dunite Fragment in Meteorite Northwest Africa (NWA) 11421: A Piece of the Moon's Mantle

REVISION 1

Word Count = 5100, plus 1782 in appendices.

Allan H. Treiman[1], Julia Semprich[2]

[1] Lunar and Planetary Institute, 3600 Bay Area Boulevard, Houston, TX 77058 <treiman@lpi.usra.edu>

[2] AstrobiologyOU, School of Environment, Earth and Ecosystem Sciences, The Open University, Walton Hall, Milton Keynes MK7 6AA, UK julia.semprich@open.ac.uk

Abstract

A centimeter-sized fragment of dunite, the first recognized fragment of Moon mantle material, has been discovered in the lunar highlands breccia meteorite Northwest Africa (NWA) 11421. The dunite consists of 95% olivine (Fo_{83}), with low-Ca and high-Ca pyroxenes, plagioclase, and chrome spinel. Mineral compositions vary little across the clast, and are consistent with chemical equilibration. Mineral thermobarometry implies that the dunite equilibrated at 980±20°C and 0.4±0.1 Gigapascal (GPa) pressure. The pressure at the base of the Moon's crust (density 2550 kg/m^3) is 0.14-0.18 GPa, so the dunite equilibrated well into the Moon's upper mantle. Assuming a mantle density of 3400 kg/m^3, the dunite equilibrated at a depth of 88±22 km. Its temperature and depth of equilibration are consistent with the calculated present-day lunar geotherm (i.e., selenotherm).

The dunite's composition, calculated from mineral analyses and proportions, contains less Al, Ti etc. than chondritic material, implying that it is of a differentiated mantle (including cumulates from a lunar magma ocean). The absence of phases containing P, Zr, etc. suggests minimal involvement of a KREEP component, and the low proportion of Ti suggest minimal interaction with late melt fractionates from a lunar magma ocean. The Mg/Fe ratio of the dunite (Fo_{83}) is significantly lower than models of an overturned unmixed mantle would suggest, but is consistent with estimates of the bulk composition of the Moon's mantle.

Key words: Moon, mantle, dunite, meteorite, thermobarometry, NWA 11421, selenotherm

Introduction

The Moon's mantle forms the greatest portion (by volume and mass) of the Moon, and figures prominently in all models of the Moon's origin and evolution (Shearer and Papike, 1999; Elkins-Tanton et al., 2002b; Wieczorek et al., 2006; Wieczorek et al., 2013). Until now, understanding of the lunar mantle has been hindered by the absence of samples of mantle material. Lacking lunar mantle material to examine, the composition and physical state of the Moon's mantle have been inferred from geophysical data and physico-chemical models: Apollo-era seismology (Kuskov and Kronrod, 2009; Zhao et al., 2012; Matsumoto et al., 2015; Garcia et al., 2019); GRAIL measurements of gravity (Wieczorek et al., 2006; Matsuyama et al., 2016); and theoretical models based on those constraints and estimates of the Moon's bulk composition (Elkins-Tanton et al., 2002a; Wieczorek et al., 2006; Elkins-Tanton et al., 2011). Here, we present the first undisputable sample of the lunar mantle, and its implications for its origin.

Lunar Evolution: Background

The standing model of the evolution of the lunar mantle starts as a planet-encompassing lunar magma ocean (LMO), produced during a collision between the proto-Earth and a planetesimal (Wieczorek et al., 2006; Elkins-Tanton et al., 2011). As the LMO cooled, it crystallized mafic minerals, olivine followed by low-Ca pyroxene and then augite, which sank to form cumulate igneous rocks at the base of the ocean. The minerals became more ferroan (less magnesian) as crystallization proceeded. The mafic minerals accumulated in a chemically and mineralogically layered pile. Plagioclase was among the last minerals to crystallize, and it floated on the remaining LMO to form an anorthositic crust (Wood et al., 1970; Elkins-Tanton et al., 2011; Wieczorek et al., 2013). The last dregs of the LMO were rich in incompatible elements, titanium, and iron (the KREEP component), and were denser than the underlying mafic cumulates (Srivastava et al., 2022). The whole mantle was gravitationally unstable, with denser, ferroan material overlying lighter, magnesian material. Under the influence of gravity, the mantle overturned, bringing magnesian cumulates toward the surface and ferroan and Ti-rich materials to depth (Hess and Parmentier, 1995; Elkins-Tanton et al., 2011). The overturned mantle could have been chemically layered, with the original stratigraphy essentially intact but inverted (Elkins-Tanton et al., 2011). Alternatively, the overturned mantle could have been mixed to various degrees (Boukaré et al., 2018; Zhao et al., 2019; Moriarty et al., 2021; Schwinger and Breuer, 2022). For a detailed summary see Gross and Joy (2016).

The lunar crust, originally the plagioclase flotation cumulates, is less than 45 km thick as calculated from gravity and seismic data (Wieczorek et al., 2013). It is reasonable that larger impact basins would have penetrated the crust and exposed and/or excavated lunar mantle material (Morrison, 1998; Potter et al., 2012; Vaughan et al., 2013; Miljković et al., 2015; Moriarty et al., 2021). Many outcrops of olivine rich material have been identified around lunar basins, and could represent uplifted mantle material (Nakamura et al., 2009; Yamamoto et al., 2010; Klima et al., 2011; Kramer et al., 2013; Moriarty et al., 2013; Corley et al., 2018; Gou et al., 2019; Lemelin et al., 2019; Li et al., 2019; Bretzfelder et al., 2020; Gou et al., 2020; Moriarty III et al., 2021). However, mineralogy and mineral compositions determined by remote sensing do not permit determination of pressures and temperatures of equilibration.

Lunar Dunites:

Returned Samples

There are few dunites and peridotites in the returned lunar sample collection. Only one macroscopic dunite was collected by the Apollo astronauts, 72415 (and its pairs), and peridotitic fragments are known in only a few lunar breccia rocks.

The only large sample of lunar dunite, 72415 to 72418, was a clast in a fragmental melt breccia, exemplified by sample 72435 (Meyer Jr, 2012). 72415 is a cataclastic breccia, composed primarily of olivine fragments (up to 10 mm across) in a matrix of granulated olivine with small proportions of high- and low-Ca pyroxenes, plagioclase, chromite, and others (Dymek et al., 1975). 72415 has been interpreted as nearly monomict, with rare fragments of chromite-pyroxene symplectites and impactites (Dymek et al., 1975). Olivine in 72415 has a small range in composition, Fo_{86-89} (the Fo number is atomic Mg/(Mg+Fe) in %, see Table 1), and two-pyroxene thermometry implies equilibration at 1120°C (Ishii et al., 1976). The source of 72415 (mantle or crust) is discussed below.

Approximately a dozen fragments of dunite and peridotite have been recognized in Apollo 14 breccias (Taylor and Marvin, 1971; Lindstrom et al., 1984; Shervais et al., 1984; Goodrich et al., 1986; Warren et al., 1987; Morris et al., 1990; Snyder et al., 1995; Shervais and McGee, 1999). These olivine-rich rocklets are all magnesian and variably enriched in KREEP component. For the most part, they have been interpreted as crustal cumulates from Mg-suite magmas. The Apollo 14 breccias also contain a few complex peridotitic fragments, one of which is interpreted as asteroidal (Shervais et al., 1984). The others are likely to be fragments of crustal cumulate rocks (Taylor and Marvin, 1971; Morris et al., 1990).

A few dunite fragments are reported from Apollo 15 regolith breccias (Marvin et al., 1989b, a, 1991). Marvin and colleagues suggested that these fragments formed at significant depth, but did not distinguish between a crustal and mantle origin.

Finally, the Apollo 17 basalt 74275 contains xenoliths of dunite (Shearer et al., 2015a). The xenoliths' olivines' cores retain igneous-like zoning patterns in Al, Ti, and P; this zoning led Shearer et al. to infer a shallow crustal origin. However, similar chemical zoning has recently been recognized in the troctolite 76535 (Nelson et al., 2021), which is inferred to have formed at depth and cooled slowly, see Fig. 4 here and McCallum and Schwartz (2001).

Meteorites

Among lunar meteorites, only a few dunitic and peridotitic clasts have been reported in regolith or melt breccias; no lunar meteoritic dunites (or dunitic peridotites) are known. In meteorite ALH 81005, despite extensive study of many thin sections, only a few peridotitic fragments have been reported (Kurat and Brandstätter, 1983; Warren et al., 1983; Brum, 2022; Brum et al., 2022). Dunitic and peridotitic material are absent to uncommon in other lunar meteorites (Warren et al., 1983; Arai et al., 2002; Nazarov et al., 2004; Sugihara et al., 2004; Hudgins et al., 2007; Bischoff et al., 2010; Mercer et al., 2013; Cao et al., 2020; Bechtold et al., 2021). Many of these fragments have moderate Mg*, and are likely related to the lunar Mg-suite (Shearer et al., 2015b).

NWA 8046 Clan

Here, we present a clast of dunite in lunar meteorite Northwest Africa (NWA) 11421, which is a member of the NWA 8046 clan of lunar highlands breccias, the "Algerian Megafind" (Korotev, 2022). These tens of named meteorites are paired, being either all fragments of the same meteoroid fall, or being 'source paired' in coming from the same site on the Moon. The most detailed published description of NWA 8046 meteorite is for NWA 11460 by Cao et al. (2021). Their description is consistent with our observations of NWA 11421.

A dunite clast is also present in NWA 14900 (Sheikh et al., 2022), a member of the NWA 8046 clan (Korotev, 2022). This fragment consists only of olivine (Fo_{91}) with a miniscule proportion of chromite. No other studies of NWA 8046 meteorites mention clasts of dunite, peridotite, or other ultramafic materials (Lunning and Gross, 2019; Fagan and Gross, 2020; Zeng et al., 2020; Treiman and Semprich, 2021; Saini et al., 2022).

Samples and Methods

Samples

A piece of NWA 11421, 11.67 gram, was purchased from M. Cimala of Polandmet.com (Figure 1). The properties of this fragment are consistent with the official description of the meteorite (Gattacceca et al., 2018). NWA 11421 a member of the NWA 8046 clan of impact melt breccias, which consist of mineral and lithic fragments (mostly anorthositic troctolite or lherzolite) in dense black glass, see Figure 1 (Treiman and Coleff, 2018; Cao et al., 2021; Korotev, 2022). The dunite clast studied here, D1 (Fig. 1), was noted on a weathered surface by its color, and its extent determined with X-ray computed tomography, XCT, see Figure 2 (Treiman and Coleff, 2018). Based on the XCT, the sample was cut to produce two thick sections (labelled NWA 11421_lpi1 and _lpi2) that expose the dunite clast (NWA 11421_lpi1_D1), leaving a significant portion of it remaining in the meteorite fragment. The results here are all from NWA 11421_lpi1.

Methods

Electron Microbeam. The dunite D1 and its surroundings in thick section NWA 11421_lpi1 were imaged in backscattered electron (BSE) mode using the JEOL 7600F at the Astromaterials Research and Exploration Science (ARES) Division, Johnson Space Center, Houston TX and with the PhenomXL© SEM at the Lunar and Planetary Institute (USRA), Houston TX. Qualitative maps of element abundances (by energy dispersive spectrometry, EDS), were acquired with the same instruments. Based on these element mappings, selected spots were chosen for quantitative chemical analysis using the JEOL 8530 FEG electron microprobe (EMP) at ARES. Analytical conditions were nominal for the instrument and laboratory. Peak intensities were measured for Kα radiation of these elements using well-characterized standards: Si, diopside; Ti, rutile; Al, oligoclase; Cr, chromite; Fe, fayalite; Ni, NiO; Mn, rhodonite; Mg, diopside or forsterite; Ca, diopside; Na, oligoclase; K, orthoclase; and S, anhydrite. The incident electron beam was at 15 kV and 10 nA (for plagioclase) or 25 nA (for other minerals) measured into a Faraday cup, and was focused on surfaces of standards and samples. Peak X-ray intensities were counted for 30-60 seconds, and backgrounds were counted for the same total durations. Analytical standards were run as unknowns to validate the calibrations.

All mineral analyses and their locations on the thick section are given in the Supplemental Material.

Mineral proportions, Densities, & Bulk composition. Mineral proportions in the dunite clast D1 were calculated using a supervised classification routine on element abundance images from the SEM. The classification was done using the Multispec© program (Landgrebe and Biehl, 2011) following the protocols of Maloy and Treiman (2007). X-ray element images were masked to include only the D1 clast; mineral classification training was based on EMP quantitative point analyses. Mineral densities (at 1 bar) were calculated assuming linear mixing from the densities of end-member compositions.

D1's bulk composition was calculated from the area proportion of each phase in it (olivine, orthopyroxene, clinopyroxene, plagioclase, chromite), the point EMP analyses of each phase, and the calculated densities of each.

X-ray Computed Tomography (XCT). An X-ray tomography image stack of the whole meteorite piece was acquired at the ARES division of Johnson Space Center in May 2018 (Treiman and Coleff, 2018). The XCT instrumentation and methods are as described in Zeigler et al. (2017) and Eckley et al. (2020); see Appendix I.

Thermobarometry. Details of the thermobarometry calculations, including mineral analyses on which they are based, are given in the text below and in Appendix II.

Results

The analyzed section of NWA 11421 is a lunar highlands melt breccia (Figs. 1, 2, 3) consistent with its classification (Gattacceca et al., 2018) and its pairing into the NWA 8046 clan (Korotev, 2022). Most of the lithic fragments in the section are troctolitic or lherzolithic anorthosites (Fig. 2d, 3a); there are also clasts of anorthositic impact melt and breccia. No basaltic or KREEPy fragments have been noted, although the rock contains rare small fragments of evolved, silica-rich material (Treiman and Semprich, 2019). Mineral grains include those from the anorthositic and dunitic lithologies, and other types including exsolved low-Ca and high-Ca pyroxenes, Fe-sulfide, Fe-metal, and Mg-Al spinel (Fig. 3a).

The thick section _lpi1 (and the meteorite in general) shows minor evidence of terrestrial weathering (Korotev, 2022). One crack in the D1 dunite and its surroundings contains K-rich material, tentatively identified as clay (Fig. 3c). Another crack contains a Ca-rich grain (Fig. 3c), without other elements detectable by EMP, that is likely a Ca-carbonate. That same crack also contains a sulfur-bearing grain, again without elements detected in our EMP maps (Fig. 3c). This could be a grain of barium sulfate (barite), such as occurs in other NWA meteorites (Korotev et al., 2009).

Dunite Mineralogy and Composition

The D1 dunite fragment, before cutting, was approximately 10x7x4 mm (Figs. 1, 2). The thick section analyzed here exposes a 5x4 mm surface of the dunite (Fig 3). The thick-section surface appears representative of the whole fragment, except that it does not expose an apparent stringer of high-density material visible in the XCT scan (Fig. 2b, c).

Mineralogically, the D1 dunite is simple; it consists only of olivine, low-Ca pyroxene, high-Ca pyroxene, anorthite plagioclase, and chromite (Fig. 3a). No other phases were detected (Fig. 3), such as Fe±Ti oxides, Ca-phosphates, zircon/baddeleyite, alkali feldspar, or garnet. A small proportion of K-bearing material on a fracture (Fig. 3c) is interpreted as clay produced during terrestrial weathering. Minerals in the dunite are nearly of constant compositions and lack zoning in major or minor elements (Fig. 4); Table 1 gives average mineral compositions, and a calculated bulk composition of the dunite (based on mineral proportions, analyses, and densities; Table 2); full analyses are in the Supplemental Material.

The silicate minerals are magnesian; the olivine is Fo_{83} (Fig. 4, Table 1), and the pyroxenes are slightly more magnesian ($Wo_{03}En_{82}Fs_{15}$ and $Wo_{44}En_{49}Fs_{07}$, Table 1), consistent with Fe-Mg equilibria (Baker and Herzberg, 1980; Lindsley, 1983). The olivine has FeO/MnO = 84, consistent with a lunar provenance (Karner et al., 2003). The pyroxenes contain minor non-quadrilateral components (e.g., Al, Ti, Cr, Na), and so are represented well on a standard pyroxene quadrilateral (Fig. 4). The augite is slightly sub-calcic, and the orthopyroxene contains a small proportion of Ca (Table 1, Fig. 4). D1's plagioclase is $An_{96.5}$ (see Table 1 for values and abbreviations), such as is abundant in lunar anorthosites and most lunar rocks. Its chromite is a complex solid solution, with significant Al substitution for Cr, Mg substitution for Fe^{2+}, and a small proportion of Ti. The analytical sums for chromite are low, which we attribute to its small grain size and irregular surfaces near grain edges; the chromite standard analyzed well. It is also possible that the dunite's chromite contains an unanalyzed element or a bit of ferric iron.

This is the peer-reviewed, final accepted version for American Mineralogist, published by the Mineralogical Society of America.
The published version is subject to change. Cite as Authors (Year) Title. American Mineralogist, in press.
DOI: https://doi.org/10.2138/am-2022-8911. http://www.minsocam.org/

Mineral proportions and their calculated densities are given in Table 2, along with a calculated bulk density for the D1 dunite.

Dunite Texture

Macroscopically, the D1 dunite has a granoblastic-polygonal texture, and lacks apparent preferred mineral orientations. This absence of preferred orientations is also seen on the weathered meteorite surface (Fig. 1), in the different colors of the olivine, augite, and orthopyroxene grains. Note that the weathered and cut surfaces are approximately perpendicular to each other. Likewise, the XCT scan shows no alignments or preferred orientations of the pyroxene and plagioclase grains (Fig. 2). Thus, we infer that the dunite lacks linear and/or planar structures; i.e. it is structurally isotropic.

Olivine grains can be distinguished from each other, at least in part, by the presence of gaps (from grinding/polishing) along grain boundaries and cracks representing cleavage in individual grains (Figs. 3, 5). From this view, the D1 olivines are all of approximately the same size, ~100 μm across, and show no obvious preferred elongation direction. Boundaries between grains of olivine (as can be discerned) are generally planar (Fig. 5), and are consistent with triple-junction angles of ~120°.

Pyroxenes and plagioclases appear randomly distributed among the olivine grains, Fig. 3a, and few of these appear elongated or aligned. The few elongated augite grains (e.g., bottom left of the clast in Fig. 3a) are associated with augite-chromite symplectites and are inferred to be late-stage additions (see below). Boundaries of pyroxene and plagioclase grains against olivines are either straight or concave toward the olivine (Fig. 5), consistent with inferred constraints of equilibrium surface energy (Spry, 1969; Barker, 2013).

Symplectite

Chromite and some augite in the D1 dunite are exceptions to this textural equilibrium. Nearly all the chromite occurs either as symplectic intergrowths with augite (Figs. 5c, 5d) or elongate grains, sandwiched between silicate mineral grains. Much of the augite is in equant anhedral grains (e.g., Fig. 3a, upper right side of dunite clast), but some augite is in symplectic intergrowths with chromite (Figs. 5c, 5d), and some occurs as elongate grains between other mineral grains (e.g., at the center of Fig. 5b). The largest example of elongated grains in the thick section is in the lower left corner of the dunite in Figure 3a. There, an elongate augite grain and an augite-chromite symplectite define a short veinlet cutting the dunite. This veinlet could be an example of the high-density veinlets observed in XCT (Figs. 2b, 2c).

Inferences

Thermobarometry

The mineral compositions in the NWA 11421_lpi1_D1 dunite appear to represent a state of chemical equilibrium, so we can apply thermobarometry to determine its equilibrium temperature and pressure. We consider the minerals to be in chemical equilibrium because: the compositions of each mineral are consistent across the dunite fragment (Fig. 4 & Supplementary Material); the Mg*s of the olivine, augite, and orthopyroxene are consistent with equilibrium, see Table 1 and Figure 4 (Baker and Herzberg, 1980; Lindsley, 1983); and the Ca contents of the augite and orthopyroxene are consistent with equilibrium (Lindsley, 1983).

With this evidence of chemical equilibrium, we can apply established mineral thermobarometers to determine the temperature and pressure at which the dunite's minerals equilibrated: 980±20°C and 0.4±0.1 GPa. We calculated temperatures and pressures for six different sets of minerals (ol + pl + cpx + opx) in direct or nearly direct contact, Figure 6 (see Supplemental Material). Details of the temperature and pressure calculation are given in Appendix II. Equilibration temperatures were calculated from two-pyroxene thermometry (Ca distribution between augite and orthopyroxene) using the calibration of Brey and Köhler (1990) and two calibrations from Putirka (2008). For each set of minerals, these temperatures are within 20°C of each other. The resulting minimum and maximum temperatures were then used as input to calculate pressures using THERMOCALC's av*P* algorithm (Powell and Holland 1994, 2008), selecting the temperature that produced the P result with the lowest residuals. The calculated pressures rely primarily on the Al contents of pyroxenes, e.g., the Mg- and Ca-Tschermak's, or kushiroite (Kimura et al., 2009), components. To validate the procedure, we calculated temperatures and pressures for the lunar troctolite 76535 (Fig. 6; Appendix II); our results are comparable to those in earlier studies (McCallum and Schwartz, 2001; Elardo et al., 2012). For the six sets of minerals in the D1 dunite, calculated equilibrium temperatures range from 940 to 990°C (Fig. 6), with an average of 980°C. Calculated equilibrium pressures range from 0.27±0.1 to 0.51±0.1 GPa (Fig. 6), with a best estimate of 0.4±0.1 GPa.

Equilibration Depth – The Upper Mantle

To understand the original geologic setting of the NWA 11421_lpi1_D1 dunite, it is crucial to know how the calculated equilibrium pressure corresponds to depth. We use the Wieczorek et al. (2013) model of the lunar crust and upper mantle: a porous (fragmented) anorthositic crust with average density of 2550 kg/m^3 and thickness from 34 to 43 km, overlying a peridotitic upper mantle of density 3400 kg/m^3 (nearly identical to that calculated for the dunite, Table 2). With those constraints (and lunar surface gravity of 1.62 m/s^2), pressure at the base of the crust is calculated to be 0.14 to 0.18 GPa. The equilibration pressure for D1 is greater than these, which places D1's equilibration in the Moon's upper mantle. Using the Wieczorek et al. (2013) model, the D1 dunite equilibrated at a depth of 88±22 km, in the Moon's upper mantle.

The dunite's mineral equilibration is consistent with formation on a 'normal' present-day lunar geotherm (i.e., selenotherm), see Figure 7. Within 2σ uncertainty, the dunite's equilibration is consistent with the present-day selenotherm calculated by Khan et al. (2014) from seismic data. That seleotherm includes consideration of a partially molten mantle at depths >1200 km, and a porous crust of low thermal conductivity. The nominal pressure and temperature of equilibration plot at slightly higher temperature (or lower pressure) than Khan's selenotherm (Fig.7), consistent also with equilibration along an ancient, slightly hotter, thermal gradient.

This is the peer-reviewed, final accepted version for American Mineralogist, published by the Mineralogical Society of America.
The published version is subject to change. Cite as Authors (Year) Title. American Mineralogist, in press.
DOI: https://doi.org/10.2138/am-2022-8911. http://www.minsocam.org/

Texture

The texture of the D1 dunite (excepting the symplectites) arose during its chemical and thermal history in the moon, and so reveals some of that history. As described above, olivine grains in D1 are all of approximately the same size (Fig. 3), and show no obvious elongations or preferred orientations None of the minerals in D1 show their own crystal forms (i.e., are not idiomorphic); rather, grain boundaries are straight or curved as consistent with equilibria of mineral surface energies (Spry, 1969).

These textures of D1 are consistent with those of a granoblastic-polygonal metamorphic rock – one in which grain sizes and boundaries have adjusted to equilibrium shapes during extensive thermal metamorphism without deformation. Granoblastic-polygonal textures are common among mantle rocks from the Earth (Mercier and Nicolas, 1975), although Earth mantle rocks tend to have larger grains (e.g., ~1 mm vs the 0.1 mm of D1). Such textures are not characteristic of igneous cumulate rocks (Wager et al., 1960; Wager and Brown, 1967).

Symplectite Formation

The chromite-augite symplectites in the D1 dunite require explanation, in the context of long-standing controversies about symplectite formation in other lunar rocks. In the still-current summary, Bell et al. (1975) described six varieties of lunar symplectites, and four general formation mechanisms. The symplectites in D1 fall into Bell's category C, "… 10-1000-µm elongated masses along grain boundaries…" (Figs. 5c, d). Bell and coauthors agreed that type-C symplectites formed by reactions between olivine and plagioclase. Dymek et al. (1975) inferred that similar symplectites in 72415 formed by interaction with a silicate fluid (i.e., in an open system). Elardo et al. (2012) confirmed this inference, showing that symplectites of this type in troctolite 76535 (their Fig. 1) formed by addition of Cr and Fe in an open-system process. The D1 symplectites are similar enough to those in 76535 (Elardo et al., 2012), in texture and in composition, that a similar open system origin seems reasonable. An origin by garnet breakdown seems unlikely for the D1 symplectites, because garnet in peridotites tends to form euhedra (Spry, 1969; Dégi et al., 2010; Barker, 2013) and not intergranular pods and films (Figs. 2b, 2c, 3a, fc, 5d).

The Lunar Upper Mantle

It seems presumptuous to extrapolate from a single clast in a breccia to the Moon's whole mantle, yet such assumptions have proven useful (Wood et al., 1970). If the D1 dunite clast in NWA 11421 is representative of a portion of the lunar mantle, it could help constrain models of the Moon's early history.

The Al, Ca, and Ti abundances in the D1 dunite seem most consistent with formation in a differentiated lunar mantle that was well-mixed after its overturn (see Introduction). Estimated compositions of the bulk, undifferentiated lunar mantle have 3-7% Al_2O_3, 3-5% CaO, and 0.2 – 0.4% TiO_2 (Elkins-Tanton et al., 2011), while the dunite contains only 0.55% Al_2O_3, 0.57% CaO, and 0.07% TiO_2 (Table 1). Thus, the dunite composition is consistent (in general terms) with a primitive mantle composition that was depleted in components that partition into silicate melt (e.g., Al, Ca, Ti).

The dunite's Mg* (i.e., Fo) of 83 is consistent with most models of the bulk primitive lunar mantle, which have Mg* = 80 – 85; see Table 1 of Elkins-Tanton et al. (2011). A lunar mantle that differentiated during a magma ocean episode would retain that average bulk Mg*, and be stratified with highest Mg* at its base (according to mineral-melt element partitioning). In some models of LMO crystallization, Fo_{83} olivine of is calculated to form only after ~65-75% of LMO crystallization (depending on the model starting composition), and is nearly the last olivine to crystallize (Elkins-Tanton et al., 2011; Lin et al., 2020; Johnson et al., 2021). In other models of LMO crystallization Fo_{83} olivine does not crystallize (Snyder et al., 1992; Rapp and Draper, 2018); low-Ca pyroxene would be the only silicate with Mg*=83.

This cumulate pile from a crystallizing LMO would have been gravitationally unstable, having the Fe-rich denser materials near the top. This pile would have overturned, bringing denser material to the mantle base with some degree of mixing (Hess and Parmentier, 1995). If there had been no mixing after overturn, e.g. Figure 5b of Elkins-Tanton et al. (2011), olivine at the depth inferred for the NWA 11421 dunite

This is the peer-reviewed, final accepted version for American Mineralogist, published by the Mineralogical Society of America.
The published version is subject to change. Cite as Authors (Year) Title. American Mineralogist, in press.
DOI: https://doi.org/10.2138/am-2022-8911. http://www.minsocam.org/

would be ~Fo_{90}, significantly more magnesian than it is (Table 1). This mismatch in Fo number implies that at least some of the lunar mantle had been mixed during overturn. However, the presence of augite-chromite symplectites that post-date dunite formation (see below) allows the possibility that the original dunite might have been somewhat more magnesian than what we now see, having equilibrated with the Fe-Cr-bearing material responsible for the symplectites.

If a stratified differentiated lunar mantle had homogenized during or after overturn (Boukaré et al., 2018; Zhao et al., 2019), it would maintain its bulk Mg* across all depths and so would be consistent with the Mg* and inferred depth for the NWA 11421 dunite (Table 1). Likewise, abundances of Al and Ti in the dunite are consistent with a differentiated mantle, one from which igneous incompatible elements had been partially removed to form the lunar anorthositic crust, and incompatible-enriched late LMO melts. So, the NWA 11421 dunite is most consistent with a lunar mantle that was mixed well after (or during) its overturn (Boukaré et al., 2018; Moriarty et al., 2021).

Discussion: Other Possible Sample of the Lunar Mantle

To our knowledge, D1 in NWA 11421 is the first lunar sample known to have equilibrated at pressures consistent with the lunar mantle. It is possible that other lunar dunites and peridotites are samples of the lunar mantle, but few are reported to have mineral assemblages (olivine – plagioclase – augite – low-Ca pyoxene) that could provide equilibration temperatures and pressures (see Appendix II). See Appendix III for comments about thermobarometry of lunar spinel cataclasites.

However, many lunar symplectites have bulk compositions consistent with mixtures of garnet ± olivine (Bell et al., 1975), which suggests that they were originally those minerals, and decomposed to augite + chromite on decompression (Bell et al., 1975; Schmitt, 2016). Specifically, symplectites in dunite 72415 have been interpreted as products of the decomposition of garnet (Schmitt, 2016; Bhanot et al., 2022). If so, the garnet must have originated in the lower lunar mantle, at pressures greater perhaps than 2.3 GPa (Schmitt, 2016). The garnet would then have been transported, perhaps during the overturn of the LMO cumulates, to the shallow mantle (Bhanot et al., 2022)

This is the peer-reviewed, final accepted version for American Mineralogist, published by the Mineralogical Society of America.
The published version is subject to change. Cite as Authors (Year) Title. American Mineralogist, in press.
DOI: https://doi.org/10.2138/am-2022-8911. http://www.minsocam.org/

where it could have decomposed to symplectites and then would have been transported to the surface.

Implications

The D1 dunite clast in NWA 11421_lpi1 equilibrated last at ~980°C and 0.4±0.1 GPa, at a depth of 88±22 km, firmly in the Moon's upper mantle. This temperature and pressure are consistent with estimates of the present-day selenotherm (Khan et al., 2014). Its chemical composition (Mg*, Al content) is consistent with estimates of the bulk composition of the lunar mantle, suggesting that the dunite formed after mantle differentiation (separation of anorthositic crust and Fe-Ti-rich residua) and after density-driven overturn had re-homogenized the mantle. This interpretation of the D1 dunite's origin is not unique – a similar chemistry and texture could form from an undifferentiated mantle composition by removal of a partial melt or perhaps a garnetiferous peridotite.

The veinlets and masses of augite and augite-chromite symplectite represent a fluid-based metasomatic event, after the dunite host had achieved textural equilibrium (presumably still in the mantle). Similar metasomatic products occur in other lunar and asteroidal samples (Elardo et al. 2012) (Vaci et al., 2021), and their origin remains unclear, especially the nature and origin of the metasomatic fluid.

The D1 dunite is the first recognized sample of the lunar mantle, although mantle rock is inferred to have been brought to the surface by large impact events (Yamamoto et al., 2010; Miljković et al., 2015; Bretzfelder et al., 2020; Moriarty et al., 2021). It is puzzling that no other bits of mantle dunite have been recognized, despite the relative abundance of crustal intrusive rocks in the meteorite and Apollo collections, e.g. McCallum and Schwartz (2001) and Elardo et al. (2012). Finding other fragments of lunar mantle rock would be very useful, and the search should be widened. The clast described here was recognized first because it was exposed on a weathered surface; where possible, XCT scans of other lunar breccias could reveal more fragments of the lunar mantle.

Acknowledgments

We are grateful to M. Cimala for availability of the meteorite sample, and for providing the original of Figure 1. We are grateful to K. Ross for assistance with the EMP analyses, and to C. Goodrich for some of those analyses. D. Coleff and R. Zeigler assisted with the XCT scan. The Phenom© SEM at the Lunar and Planetary Institute (LPI) was purchased with funds from USRA's IR&D fund. The LPI is operated by Universities Space Research Association (USRA) under a cooperative agreement with the Science Mission Directorate of NASA. The thick section NWA 11421_lpi1 with the dunite clast D1 is curated at the XSPACE archive at the Lunar and Planetary Institute (https://www.lpi.usra.edu/science/science-labs-equipment/xspace/). Reviewer comments and corrections from J. Gross, A. Ruzicka, D. Shiekh, H. Downes, and an anonymous reviewer are deeply appreciated. LPI Contribution #2xxx.

TABLES

Table 1. Average Mineral Compositions, and Calculated Bulk Composition for the D1 Dunite.

	Olivine	OPX	Augite	Chromite	Plagioclase	Dunite Bulk
analyses	29	15	18	3	3	Calculated
SiO_2	39.86 ± 0.22	55.17 ± 0.67	52.16 ± 0.52	0.56 ± 0.56	44.02 ± 0.49	39.65 ± 0.23
TiO_2	0.04 ± 0.01	0.58 ± 0.06	1.14 ± 0.22	1.61 ± 0.25	0.01 ± 0.01	0.07 ± 0.01
Al_2O_3	0.06 ± 0.12	1.51 ± 0.23	2.20 ± 0.50	11.20 ± 1.28	35.90 ± 0.43	0.53 ± 0.14
Cr_2O_3	0.04 ± 0.02	0.60 ± 0.04	0.82 ± 0.09	50.96 ± 3.45	0.00 ± 0.00	0.51 ± 0.05
FeO	16.05 ± 0.15	10.08 ± 0.36	4.40 ± 0.24	26.49 ± 0.92	0.69 ± 0.07	15.72 ± 0.16
MnO	0.19 ± 0.01	0.20 ± 0.01	0.12 ± 0.01	0.41 ± 0.01	0.01 ± 0.01	0.18 ± 0.01
MgO	44.54 ± 0.61	30.74 ± 0.39	17.06 ± 0.40	5.46 ± 0.73	0.11 ± 0.02	43.08 ± 0.60
CaO	0.09 ± 0.22	1.41 ± 0.16	21.69 ± 0.55	0.38 ± 0.23	19.20 ± 0.03	0.48 ± 0.22
Na_2O	0.00 ± 0.00	0.01 ± 0.01	0.06 ± 0.01	0.00 ± 0.00	0.38 ± 0.00	0.01 ± 0.00
total	100.87 ± 0.48	100.31 ± 0.50	99.65 ± 0.65	97.09 ± 1.72	100.33 ± 1.00	100.23 ± 0.23
Molar	Olivine	OPX	Augite	Chromite	Plagioclase	Dunite Bulk
Cations	3	4	4	3	5	Calculated
Si	0.996	1.939	1.917	0.020	2.030	
Ti	0.001	0.015	0.032	0.042	0.000	
Al	0.002	0.063	0.096	0.459	1.952	
Cr	0.001	0.017	0.024	1.400	0.000	
Fe	0.335	0.296	0.135	0.770	0.026	
Mn	0.004	0.006	0.004	0.012	0.000	
Mg	1.659	1.610	0.935	0.283	0.008	
Ca	0.002	0.053	0.854	0.014	0.949	
Na	0.000	0.000	0.004	0.000	0.034	
Mg*	83.2	84.5	87.4	26.9		83.1
Wo		2.7	44.4			
En		82.2	48.6			
Fs		15.1	7.0			
An					96.5	

See Supplemental Material spreadsheet for details and individual analyses. Uncertainties are 1σ.
Mg* is molar Mg/(Mg+Fe) in %; In pyroxenes, Wo is molar proportion CaSiO (molar % Ca/(Ca+Mg+Fe)), and En is molar proportion $MgSiO_3$ (molar % Mg/(Ca+Mg+Fe)).
An is molar Ca/(Ca+Na) in %.

Table 2. Mineral Proportions and Densities

Mineral	Area %	Density kg/m^3
Olivine	95.3	3380
Augite	1.1	3250
Orthopyroxene	1.6	3400
Plagioclase	1.3	2730
Chromite	0.7	5000
Bulk Dunite		3380

This is the peer-reviewed, final accepted version for American Mineralogist, published by the Mineralogical Society of America.
The published version is subject to change. Cite as Authors (Year) Title. American Mineralogist, in press.
DOI: https://doi.org/10.2138/am-2022-8911. http://www.minsocam.org/

Figures & Captions

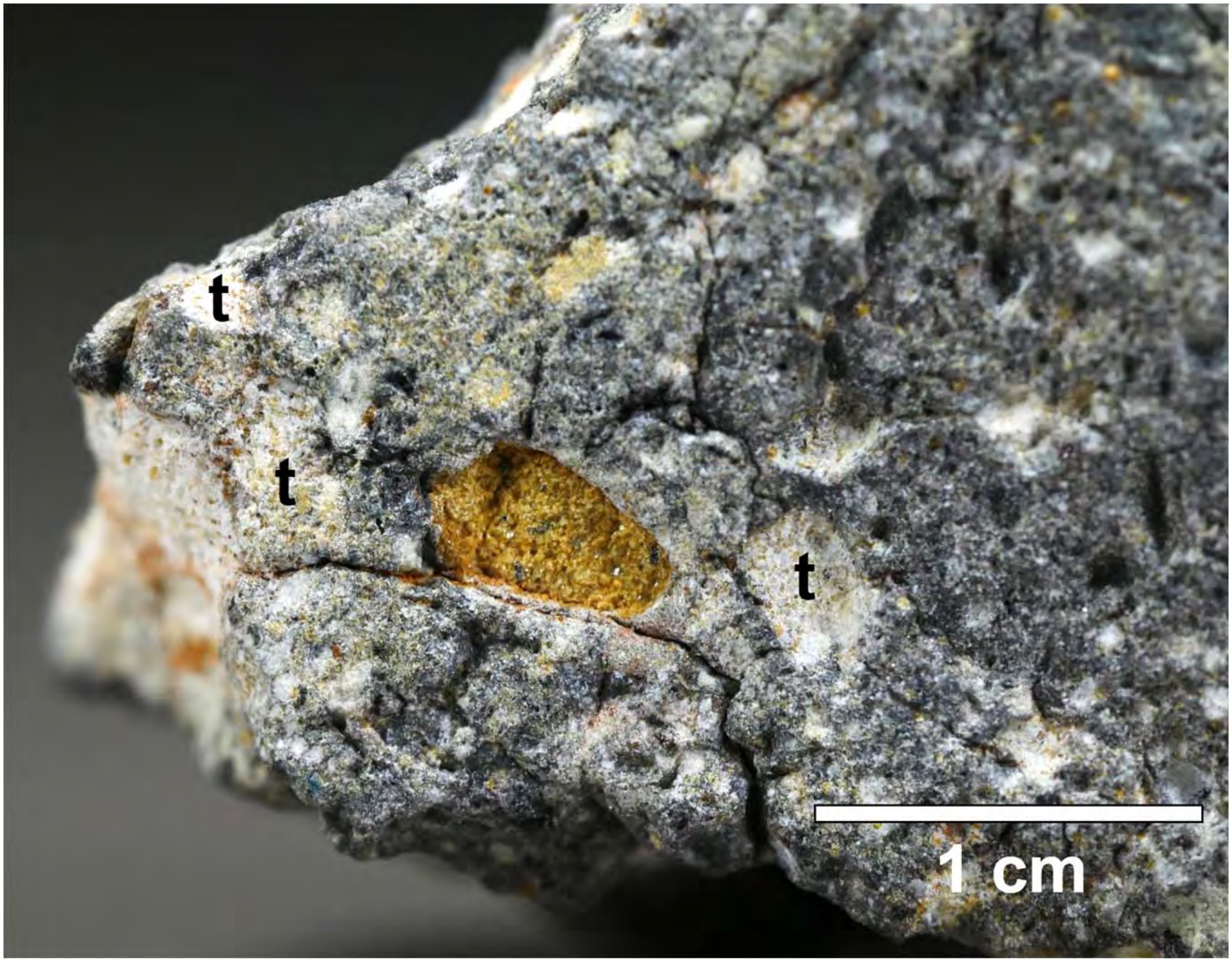

Figure 1. A portion of the NWA 11421 fragment investigated here, macroscopic visible-light, true color. The meteorite consists of lithic clasts in dark glassy matrix. The studied dunite clast (D1) at the image center is brown, 0.7 cm long. In it, olivine is pale brown, orthopyroxene is darker brown, and augite is dark green. Most other visible clasts are troctolitic (t, plagioclase + olivine). Photo courtesy of M. Cimala (polandmet.com).

DOI: https://doi.org/10.2138/am-2022-8911. http://www.minsocam.org/

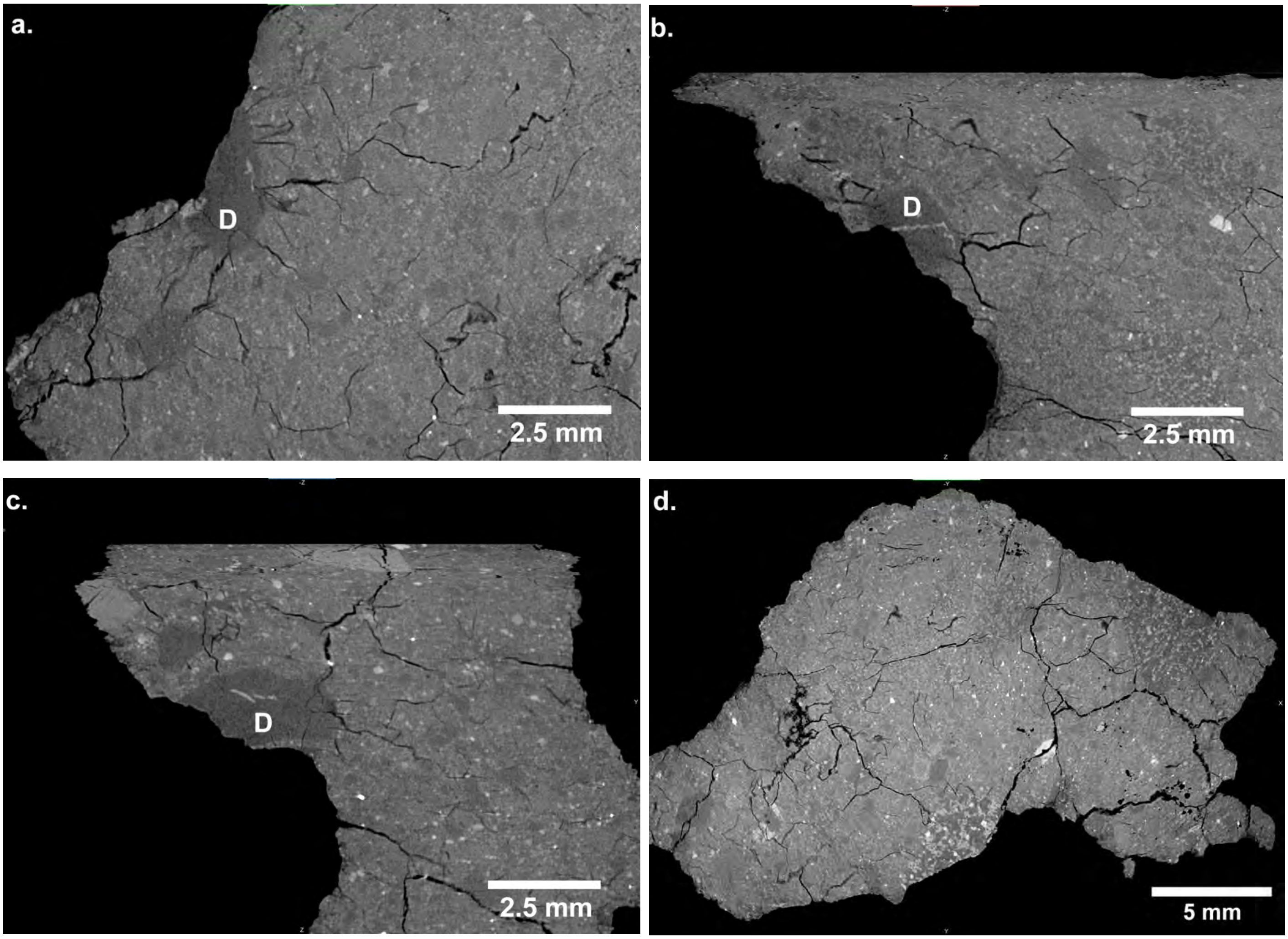

Figure 2. X-ray computed tomogram (XCT) slices of the NWA 11241 piece. a. Parallel to the base of the sample (in Fig. 1), cutting through the dunite clast (D). Note other dark, plagioclase-rich clasts and speckled matrix (devitrified impact melt). b. XCT slice perpendicular to that of 1a, bottom of the sample to top of image, & partially distorted. Dunite (D) cut by bright veinlet, possibly rich in chromite symplectite. c. XCT slice perpendicular to those of 1a & 1b, bottom of the sample to top of image, & partially distorted. Dunite (D) cut by bright discontinuous veinlets. d. General XCT view of meteorite, slice parallel to that of Fig. 1a, but away from the dunite. Note coarser grained clasts of plagioclase-rich (dark areas) troctolite and lherzolite in fine-grained speckled matrix (devitrified impact melt).

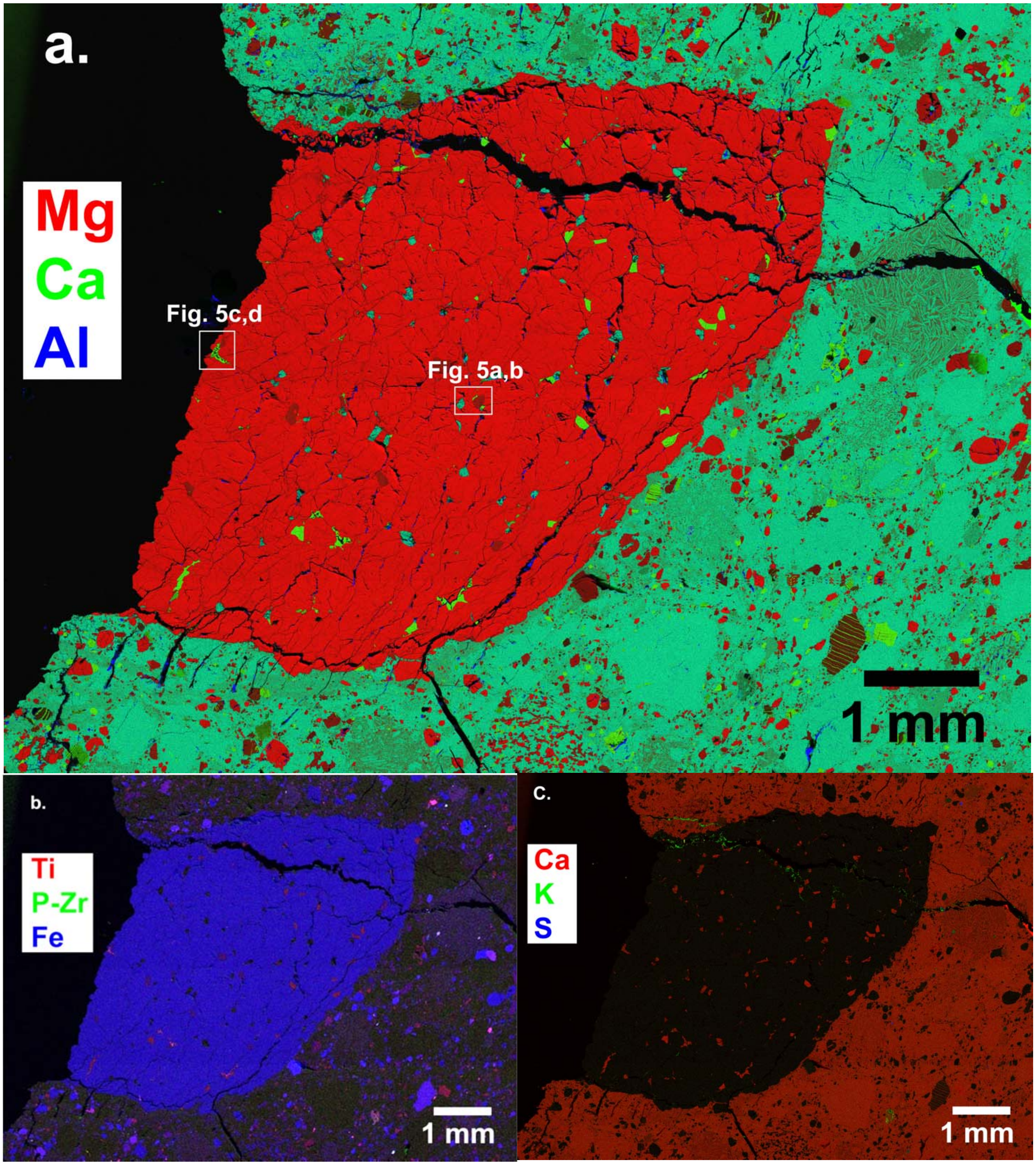

Figure 3. Multi-element images, by SEM/EDS of the D1 dunite clast and surroundings. Epoxy is black in all frames (left of the rock sample, and filling cracks across it. **a.** Mg-Ca-Al, showing main minerals in clast, and their chemical homogeneity. In the dunite clast: bright red is olivine; dull red is orthopyroxene; green is augite; blue-green is plagioclase, and small discrete black spots in the dunite are chromite. White rectangles are locations of images in Figure 5. The matrix, being rich in plagioclase, is dominantly blue-green. **b.** Ti-P(Zr)-Fe. PKα and ZrLα X-rays are not distinguished. The dunite and many mineral fragments in the matrix contain Fe (in blue). Chromite in the dunite is magenta, as is ilmenite in the matrix. A few spots in the matrix, greenish and white, could be Ca-phosphate, zircon, or baddeleyite. **c.** Ca-K-S, shows weathering products along cracks. Ca-rich spots along a crack (bright red, far right center) are interpreted as calcite; K-bearing streaks and veinlets (green) are interpreted as clay minerals. A few S-rich grains (blue) along cracks (S, but no

This is the peer-reviewed, final accepted version for American Mineralogist, published by the Mineralogical Society of America.
The published version is subject to change. Cite as Authors (Year) Title. American Mineralogist, in press.
DOI: https://doi.org/10.2138/am-2022-8911. http://www.minsocam.org/

Ca) could be barite; S-rich spots in the matrix are Fe-sulfides. The small greenish clast (K-bearing) left of the scale bar is one of the few evolved rock fragments in the meteorite (Treiman and Semprich, 2021).

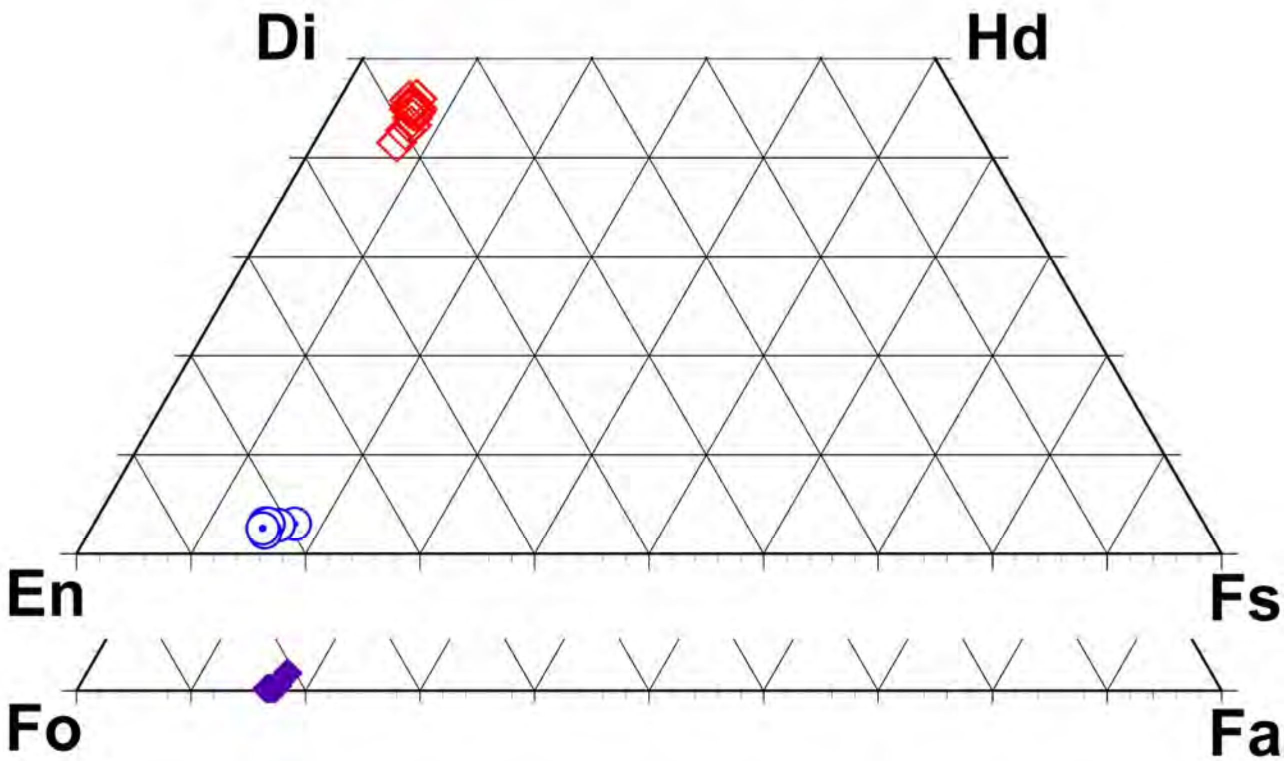

Figure 4. Pyroxene and olivine compositions in the D1 dunite. Pyroxene end-members are: En = enstatite ($Mg_2Si_2O_6$); Fs = ferrosilite ($Fe_2Si_2O_6$); Di = diopside ($CaMgSi_2O_6$); Hd =hedenbergite ($CaFeSi_2O_6$). Olivine end-members are: Fo = forsterite (Mg_2SiO_4); Fa = fayalite (Fe_2SiO_4); Ca-olivine (Ca_2SiO_4). Compositions of augite (open red squares), orthopyroxene (dotted blue circles), and olivine (filled purple diamonds) are nearly constant across the dunite clast. The range of Wo content of the augite could represent slight mixture with orthopyroxene.

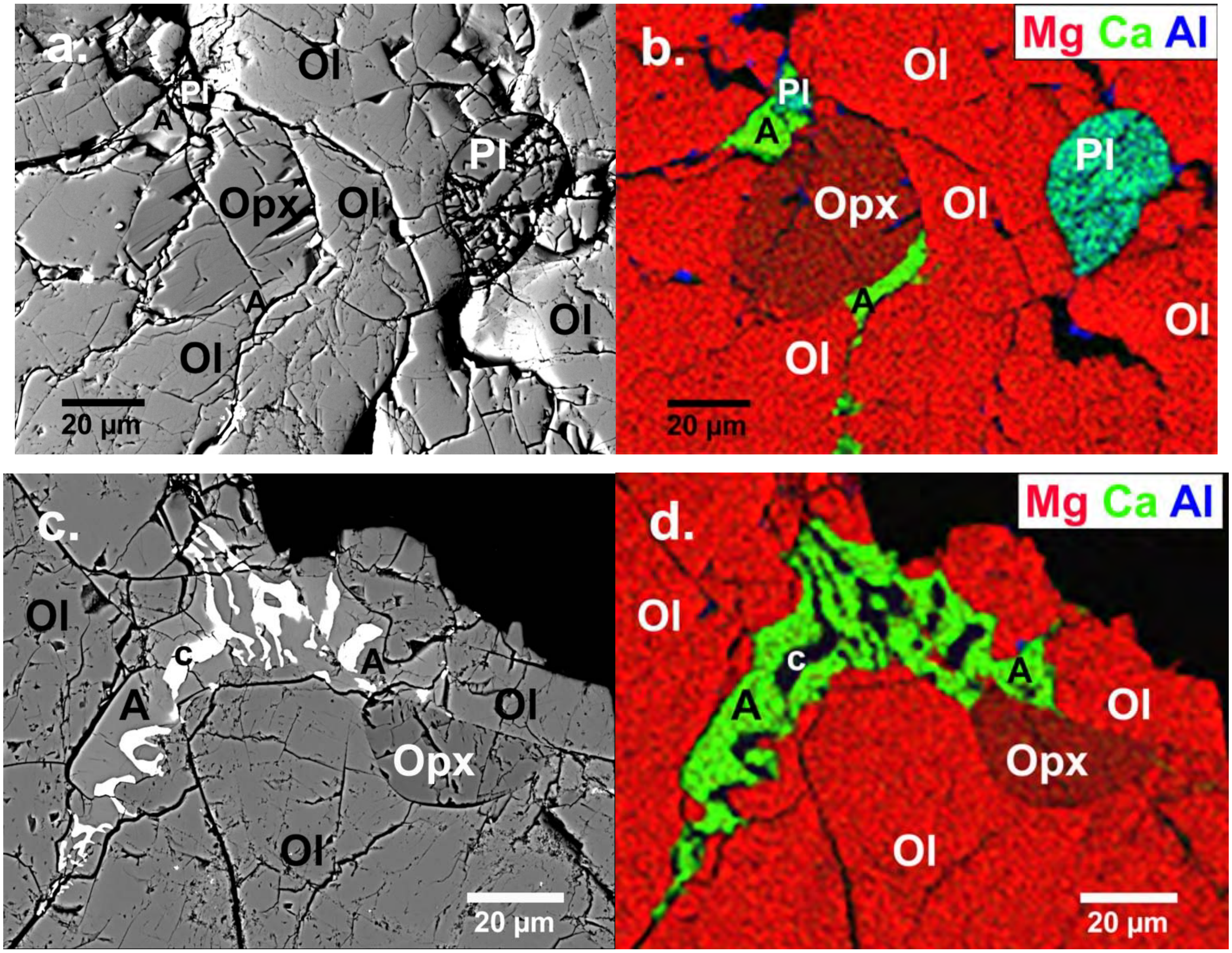

Figure 5. Details of textural relationships in the D1 dunite. **a.** BSE image of typical dunite texture: olivine (Ol, bright red), plagioclase (Pl, teal), augite (A, green), and orthopyroxene (Opx, dull red). The individual grains are in textural equilibrium, except for the elongate augite (see Fig. 5c & 5d). **b.** Mg-Ca-Al element map of same area. Enlarged by interpolation from Fig. 3a. Al-rich areas (bright blue) are traces of alumina polishing compound in cracks. **c.** BSE image of largest augite-chromite symplectite; mineral labels as above plus chromite (c). **d.** Mg-Ca-Al element map of same area as Fig. 5c. Enlarged by interpolation from Fig. 3a.

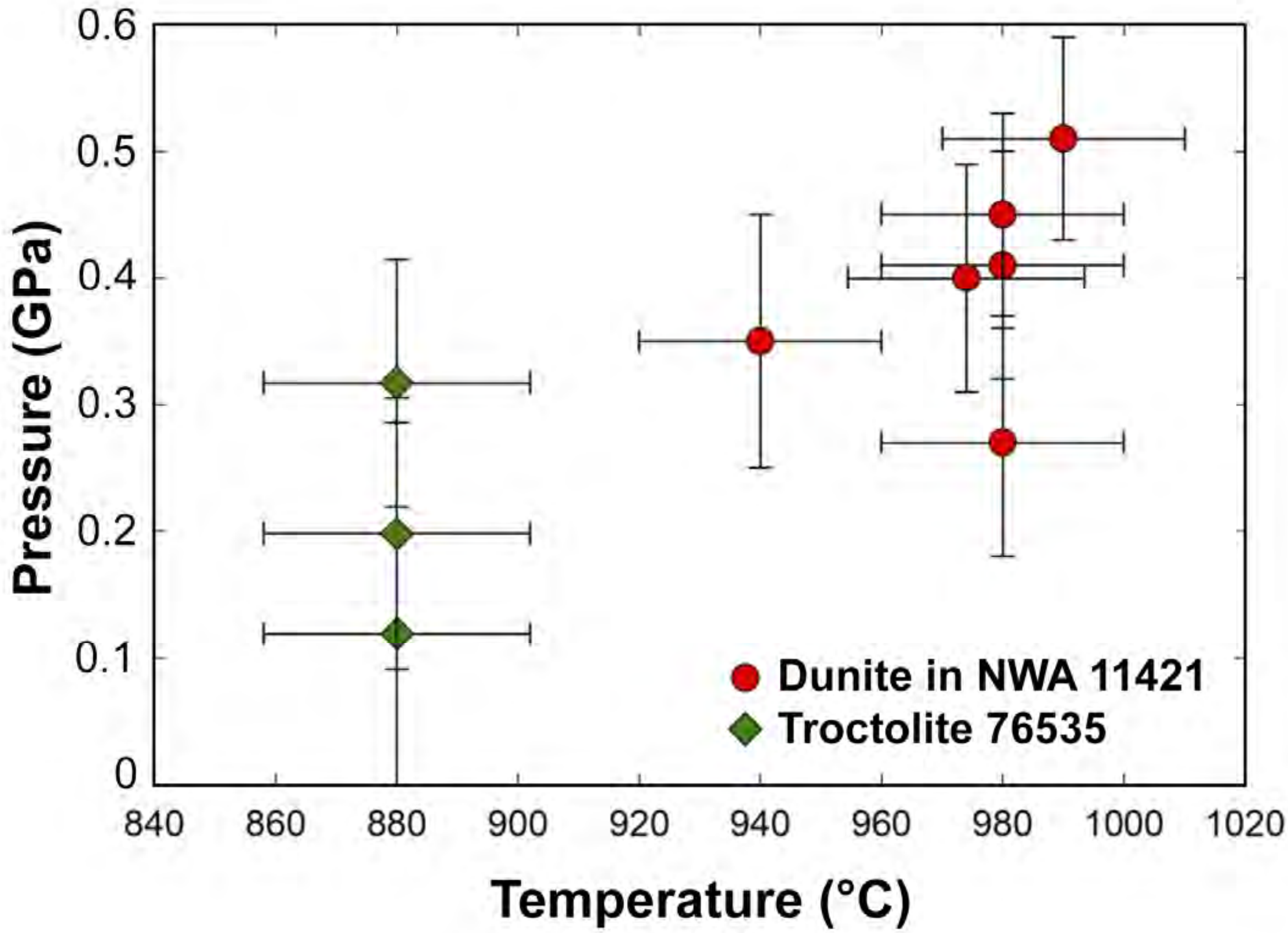

Figure 6. Calculated temperatures and pressures for separate mineral groups in the D1 dunite, red circles (see Appendix II and Supplemental Material) and clinopyroxene-olivine pairs in lunar troctolite 76535, green diamonds (see Appendix II). Standard deviations are 1σ.

DOI: https://doi.org/10.2138/am-2022-8911. http://www.minsocam.org/

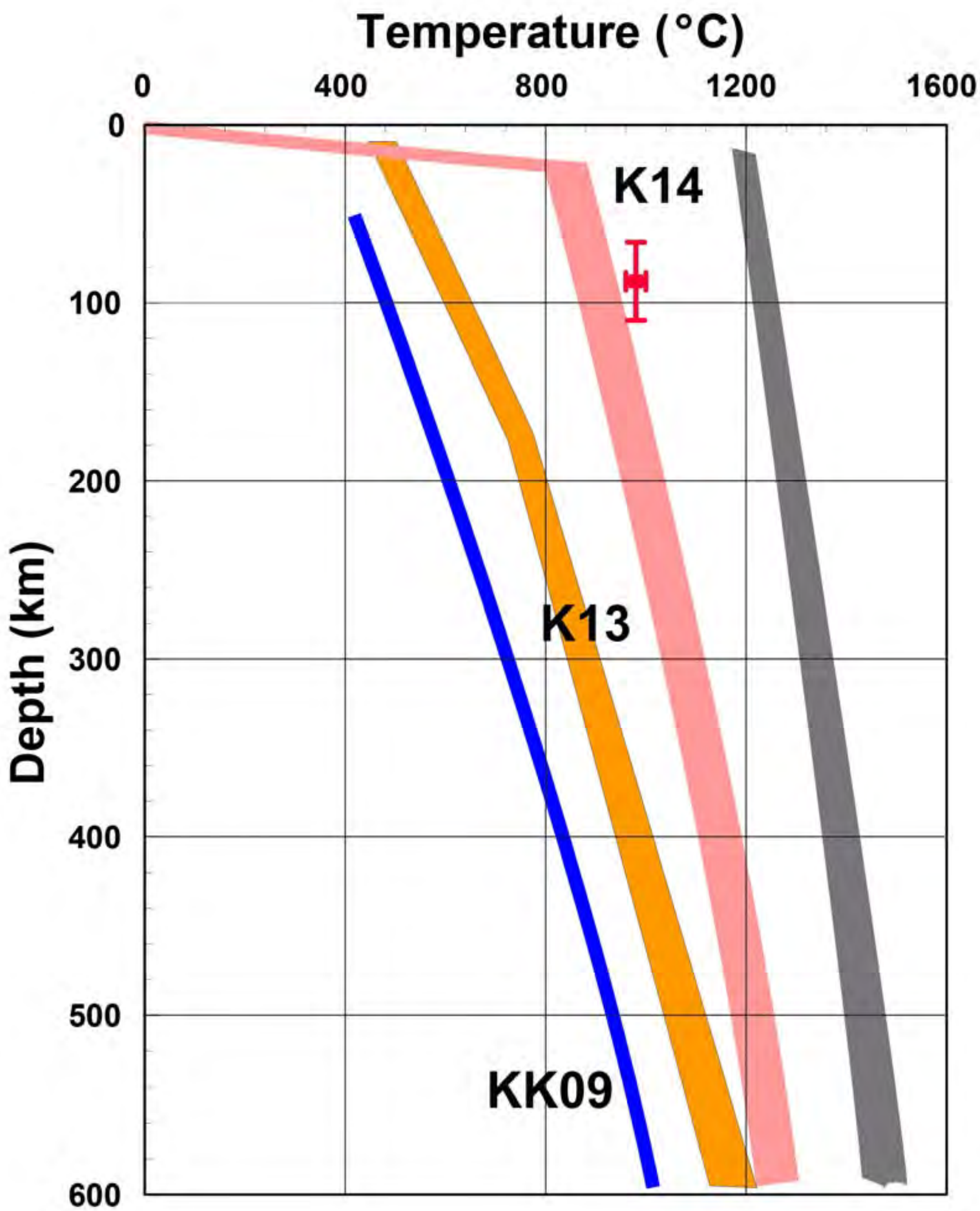

Figure 7. Equilibration conditions of the NWA 11421_lpi1_D1 dunite, and present-day thermal trajectories in the lunar mantle, after Fig. 2 of Garcia et al. (2019). Equilibrium p-T in red (Fig. 6), with 1σ uncertainties. Pink band (K14) covers best model seleotherms of Khan et al. (2014), which include 40 km thick, porous crust of low thermal conductivity. Orange band (K13) includes calculated selenotherms for dry olivine ± orthopyroxene from Karato (2013); Blue line (KK09) is selenotherm from Kuskov and Kronrod (2009). Gray band includes estimates of the solidus for undifferentiated lunar mantle material (Longhi, 2006) (Hirschmann, 2000).

clast, spinel + augite + low-Ca-pyroxene, lacks olivine and so has limited significance for calculating pressure (Herzberg and Baker, 1980) (McCallum and Schwartz, 2001) (Nazarov et al., 2011).

REFERENCES

Anderson, A.T. (1973) The texture and mineralogy of lunar peridotite, 15445,10. The Journal of Geology, 81(2), 219-226.

Arai, T., Ishi, T., and Otsuki, M. (2002) Mineralogical study of new lunar meteorite Yamato 981031. Lunar and Planetary Science Conference 33rd, 33, p. 2064.pdf.

Baker, M.B., and Herzberg, C.T. (1980) Spinel cataclasites in 15445 and 72435 - Petrology and criteria for equilibrium. Lunar and Planetary Science Conference Proceedings, 11, p. 535-553.

Barker, A.J. (2013) Introduction to Metamorphic Textures and Microstructures. Stanley-Thornes, Cheltenham, England.

Bechtold, A., Brandstätter, F., Pittarello, L., Ferrière, L., Greenwood, R.C., and Koeberl, C. (2021) Lunar meteorite Northwest Africa 11962: A regolith breccia containing records of titanium - rich lunar volcanism and the high alkali suite. Meteoritics & Planetary Science, 56(5), 971-991.

Bell, P.M., Mao, H.K., Roedder, E., and Weiblen, P.W. (1975) The problem of the origin of symplectites in olivine-beating lunar rocks. Proceedings, Lunar Science Conference 6th, p. 231-248.

Bhanot, K.K., Downes, H., Jennings, E., and Wotton, S. (2022) Apollo 17 Sample 72415 — A Fragment of the Lunar Mantle? 53rd Lunar and Planetary Science Conference, p. Abstract #1820. Lunar and Planetary Institute, Houston.

Bischoff, A., Horstmann, M., Pack, A., Laubenstein, M., and Haberer, S. (2010) Asteroid 2008 TC3– Almahata Sitta: A spectacular breccia containing many different ureilitic and chondritic lithologies. Meteoritics & Planetary Science, 45(10 - 11), 1638-1656.

Boukaré, C.-E., Parmentier, E., and Parman, S. (2018) Timing of mantle overturn during magma ocean solidification. Earth and Planetary Science Letters, 491, 216-225.

Bretzfelder, J.M., Klima, R.L., Greenhagen, B.T., Buczkowski, D.L., Petro, N.E., and Day, M. (2020) Identification of potential mantle rocks around the lunar Imbrium basin. Geophysical Research Letters, 47(22), e2020GL090334.

Brey, G.P., and Köhler, T. (1990) Geothermobarometry in four-phase lherzolites II. New thermobarometers, and practical assessment of existing thermobarometers. Journal of Petrology, 31(6), 1353-1378.

Brum, J.T. (2022) New Insights Into the Petrogenesis of Lunar Meteorite Allan Hills 81005 (ALHA81005). Geology and Environmental Earth Science, M.S., p. 72. Miami University, Miami, Ohio.

Brum, J.T., McLeod, C.L., Shaulis, B.J., and Loocke, M. (2022) 40 years of studying Allan Hills (ALHA) 81005: What else could we possibly learn? Plenty! Lunar and Planetary Science Conference 53rd, p. 2756.pdf. LPI, Houston TX.

Cao, H., Chen, J., Fu, X., and Ling, Z. (2020) Raman and infrared spectroscopic perspectives of lunar meteorite Northwest Africa 4884. Journal of Raman Spectroscopy, 51(9), 1652-1666.

Cao, H., Ling, Z., Chen, J., Fu, X., and Zou, Y. (2021) Petrography, mineralogy, and geochemistry of a new lunar magnesian feldspathic meteorite: Northwest Africa 11460. Meteoritics & Planetary Science, 56(10), 1857-1889.

Corley, L.M., McGovern, P.J., Kramer, G.Y., Lemelin, M., Trang, D., Gillis-Davis, J.J., Taylor, G.J., Powell, K.E., Kiefer, W.S., and Wieczorek, M. (2018) Olivine-bearing lithologies on the Moon: Constraints on origins and transport mechanisms from M^3 spectroscopy, radiative transfer modeling, and GRAIL crustal thickness. Icarus, 300, 287-304.

Dégi, J., Abart, R., Török, K., Bali, E., Wirth, R., and Rhede, D. (2010) Symplectite formation during decompression induced garnet breakdown in lower crustal mafic granulite xenoliths: mechanisms and rates. Contributions to Mineralogy and Petrology, 159(3), 293-314.

Droop, G.T.R. (1987) A general equation for estimating Fe^{3+} concentrations in ferromagnesian silicates and oxides from microprobe analyses, using stoichiometric criteria. Mineralogical Magazine, 51(361), 431-435.

Dymek, R., Albee, A., and Chodos, A. (1975) Comparative petrology of lunar cumulate rocks of possible primary origin - dunite 72415, troctolite 76535, norite 78235, and anorthosite 62237. Lunar and Planetary Science Conference Proceedings, 6, p. 301-341.

Eckley, S., Zeigler, R., McCubbin, F., Needham, A., Fries, M., and Gross, J. (2020) Applicability and utility of the Astromaterials X-ray computed Tomography Laboratory at Johnson Space Center. Lunar and Planetary Science Conference.

Elardo, S.M., McCubbin, F.M., and Shearer Jr, C.K. (2012) Chromite symplectites in Mg-suite troctolite 76535 as evidence for infiltration metasomatism of a lunar layered intrusion. Geochimica Cosmochimica Acta, 87, 154-177.

Elkins-Tanton, L., Van Orman, J.A., Hager, B.H., and Grove, T.L. (2002a) Re-examination of the lunar magma ocean cumulate overturn hypothesis: Melting or mixing is required. Earth and Planetary Science Letters, 196(3-4), 239-249.

Elkins-Tanton, L.T., Burgess, S., and Yin, Q.-Z. (2011) The lunar magma ocean: Reconciling the solidification process with lunar petrology and geochronology. Earth and Planetary Science Letters, 304(3), 326-336.

Elkins-Tanton, L.T., Van Orman, J.A., Hager, B.H., and Grove, T.L. (2002b) Re-examination of the lunar magma ocean cumulate overturn hypothesis: melting or mixing is required. Earth and Planetary Science Letters, 196(3-4), 239-249.

Fagan, A.L., and Gross, J. (2020) Preliminary melt models of troctolite and anorthosite clasts within Northwest Africa 11303. Lunar and Planetary Science Conference 51st, 51, p. 2904.pdf.

Garcia, R.F., Khan, A., Drilleau, M., Margerin, L., Kawamura, T., Sun, D., Wieczorek, M.A., Rivoldini, A., Nunn, C., and Weber, R.C. (2019) Lunar seismology: An update on interior structure models. Space Science Reviews, 215(8), 1-47.

Gattacceca, J., Bouvier, A., Grossman, J., Metzler, K., and Uehara, M. (2018) The Meteoritical Bulletin, No. 106. Meteoritics & Planetary Science, 54, p. 469-471.

Goodrich, C.A., Taylor, G.J., Keil, K., Kallemeyn, G.W., and Warren, P.H. (1986) Alkali norite, troctolites, and VHK mare basalts from breccia 14304. Journal of Geophysical Research: Solid Earth, 91(B4), 305-318.

Gou, S., Di, K., Yue, Z., Liu, Z., He, Z., Xu, R., Lin, H., Liu, B., Peng, M., and Wan, W. (2019) Lunar deep materials observed by Chang'e-4 rover. Earth and Planetary Science Letters, 528, 115829.

Gou, S., Di, K., Yue, Z., Liu, Z., He, Z., Xu, R., Liu, B., Peng, M., Wan, W., and Wang, Y. (2020) Forsteritic olivine and magnesium-rich orthopyroxene materials measured by Chang'e-4 rover. Icarus, 345, 113776.

Gross, J., and Joy, K.H. (2016) Evolution, lunar: From magma ocean to crust formation. Encyclopedia of lunar science, 1-20.

Herzberg, C.T., and Baker, M.B. (1980) The cordierite-to spinel-cataclasite transition - Structure of the lunar crust. Proceedings of the Conference on the Lunar Highlands Crust, p. 113-132. Pergamon, New York.

Hess, P.C., and Parmentier, E. (1995) A model for the thermal and chemical evolution of the Moon's interior: Implications for the onset of mare volcanism. Earth and Planetary Science Letters, 134(3-4), 501-514.

This is the peer-reviewed, final accepted version for American Mineralogist, published by the Mineralogical Society of America.
The published version is subject to change. Cite as Authors (Year) Title. American Mineralogist, in press.
DOI: https://doi.org/10.2138/am-2022-8911. http://www.minsocam.org/

Hirschmann, M.M. (2000) Mantle solidus: Experimental constraints and the effects of peridotite composition. Geochemistry, Geophysics, Geosystems, 1(10).

Hudgins, J., Walton, E., and Spray, J. (2007) Mineralogy, petrology, and shock history of lunar meteorite Sayh al Uhaymir 300: A crystalline impact - melt breccia. Meteoritics & Planetary Science, 42(10), 1763-1779.

Ishii, T., Miyamoto, M., and Takeda, H. (1976) Pyroxene geothermometry and crystallization-, subsolidus equilibration temperatures of lunar and achondritic pyroxenes. Lunar and Planetary Science Conference, 7, p. 410-412. Lunar and Planetary Institute Houston, Texas.

Johnson, T., Morrissey, L., Nemchin, A., Gardiner, N., and Snape, J. (2021) The phases of the Moon: Modelling crystallisation of the lunar magma ocean through equilibrium thermodynamics. Earth and Planetary Science Letters, 556, 116721.

Karato, S.-i. (2013) Geophysical constraints on the water content of the lunar mantle and its implications for the origin of the Moon. Earth and Planetary Science Letters, 384, 144-153.

Karner, J., Papike, J.J., and Shearer Jr, C.K. (2003) Olivine from planetary basalts: Chemical signatures that indicate planetary parentage and those that record igneous setting and process. American Mineralogist, 88, 806-816.

Khan, A., Connolly, J.A., Pommier, A., and Noir, J. (2014) Geophysical evidence for melt in the deep lunar interior and implications for lunar evolution. Journal of Geophysical Research: Planets, 119(10), 2197-2221.

Kimura, M., Mikouchi, T., Suzuki, A., Miyahara, M., Ohtani, E., and Goresy, A.E. (2009) Kushiroite, CaAlAlSiO6: A new mineral of the pyroxene group from the ALH 85085 CH chondrite, and its genetic significance in refractory inclusions. American Mineralogist, 94(10), 1479-1482.

Klima, R.L., Pieters, C.M., Boardman, J.W., Green, R.O., Head III, J.W., Isaacson, P.J., Mustard, J.F., Nettles, J.W., Petro, N.E., and Staid, M.I. (2011) New insights into lunar petrology: Distribution and composition of prominent low - Ca pyroxene exposures as observed by the Moon Mineralogy Mapper (M3). Journal of Geophysical Research: Planets, 116(E6).

Korotev, R.L. (2022) Lunar Meteorite: Northwest Africa 8046 clan. Washington University St. Louis, https://sites.wustl.edu/meteoritesite/items/lm_nwa_08046_clan/.

Korotev, R.L., Zeigler, R.A., Jolliff, B.L., Irvin, A.J., and Bunch, T.E. (2009) Compositional and lithological diversity among brecciated lunar meteorites of intermediate iron concentration. Meteoritics & Planetary Science, 44(9), 1287-1322.

Kramer, G.Y., Kring, D.A., Nahm, A.L., and Pieters, C.M. (2013) Spectral and photogeologic mapping of Schrödinger Basin and implications for post-South Pole-Aitken impact deep subsurface stratigraphy. Icarus, 223(1), 131-148.

Kurat, G., and Brandstätter, F. (1983) Meteorite ALHA81005: Petrology of a new lunar highland sample. Geophysical Research Letters, 10(9), 795-798.

Kuskov, O., and Kronrod, V. (2009) Geochemical constraints on the model of the composition and thermal conditions of the Moon according to seismic data. Izvestiya, Physics of the Solid Earth, 45(9), 753-768.

Landgrebe, D., and Biehl, L. (2011) An Introduction and Reference for Multispec(C), p. 193. Purdue University, https://engineering.purdue.edu/~biehl/MultiSpec/MultiSpec_Intro_9_11.pdf.

Lemelin, M., Lucey, P.G., Miljković, K., Gaddis, L.R., Hare, T., and Ohtake, M. (2019) The compositions of the lunar crust and upper mantle: Spectral analysis of the inner rings of lunar impact basins. Planetary and Space Science, 165, 230-243.

Li, C., Liu, D., Liu, B., Ren, X., Liu, J., He, Z., Zuo, W., Zeng, X., Xu, R., and Tan, X. (2019) Chang'E-4 initial spectroscopic identification of lunar far-side mantle-derived materials. Nature, 569(7756), 378-382.

Lin, Y., Hui, H., Xia, X., Shang, S., and van Westrenen, W. (2020) Experimental constraints on the solidification of a hydrous lunar magma ocean. Meteoritics & Planetary Science, 55(1), 207-230.

Lindsley, D.H. (1983) Pyroxene thermometry. American Mineralogist, 68, 477-493.

Lindstrom, M.M., Knapp, S.A., Shervais, J.W., and Taylor, L.A. (1984) Magnesian anorthosites and associated troctolites and dunite in Apollo 14 breccias. Journal of Geophysical Research: Solid Earth, 89(S01), C41-C49.

Longhi, J. (2006) Petrogenesis of picritic mare magmas: constraints on the extent of early lunar differentiation. Geochimica et Cosmochimica Acta, 70(24), 5919-5934.

Lunning, N.G., and Gross, J. (2019) Lunar feldspathic regolith breccia with magnesium-rich components: Northwest Africa 11303. Lunar and Planetary Science Conference 50th, 50, p. 2407.pdf. LPI, Houston TX.

Maloy, A.K., and Treiman, A.H. (2007) Evaluation of image classification routines for determining modal mineralogy of rocks from X-ray maps. American Mineralogist, 92(11-12), 1781-1788.

Marvin, U., Holmberg, B., and Lindstrom, M. (1989a) Granoblastic lunar "dunites" revisited. 52nd Annual Meeting of the Meteoritical Society, p. 148.

-. (1989b) Polygonized lunar "dunites" revisted. Meteoritics and Planetary Science 24(4), 299.

-. (1991) New observations on polygonize dlunar dunites. Lunar and Planetary Science Conference 22nd, 22, p. 859-860.

Matsumoto, K., Yamada, R., Kikuchi, F., Kamata, S., Ishihara, Y., Iwata, T., Hanada, H., and Sasaki, S. (2015) Internal structure of the Moon inferred from Apollo seismic data and selenodetic data from GRAIL and LLR. Geophysical Research Letters, 42(18), 7351-7358.

Matsuyama, I., Nimmo, F., Keane, J.T., Chan, N.H., Taylor, G.J., Wieczorek, M.A., Kiefer, W.S., and Williams, J.G. (2016) GRAIL, LLR, and LOLA constraints on the interior structure of the Moon. Geophysical Research Letters, 43(16), 8365-8375.

McCallum, I.S., and Schwartz, J.M. (2001) Lunar Mg suite: Thermobarometry and petrogenesis of parental magmas. Journal of Geophysical Research: Planets, 106(E11), 27969-27983.

Mercer, C.N., Treiman, A.H., and Joy, K.H. (2013) New lunar meteorite Northwest Africa 2996: A window into farside lithologies and petrogenesis. Meteoritics & Planetary Science, 48(2), 289-315.

Mercier, J.C., and Nicolas, A. (1975) Textures and fabrics of upper-mantle peridotites as illustrated by xenoliths from basalts. Journal of Petrology, 16(1), 454-487.

Meyer Jr, C. (2012) Lunar Sample Compendium 2022. Johnson Space Center, NASA, https://curator.jsc.nasa.gov/lunar/lsc/index.cfm.

Miljković, K., Wieczorek, M.A., Collins, G.S., Solomon, S.C., Smith, D.E., and Zuber, M.T. (2015) Excavation of the lunar mantle by basin-forming impact events on the Moon. Earth and Planetary Science Letters, 409, 243-251.

Moriarty, D., Pieters, C., and Isaacson, P. (2013) Compositional heterogeneity of central peaks within the South Pole - Aitken Basin. Journal of Geophysical Research: Planets, 118(11), 2310-2322.

Moriarty, D.P., Dygert, N., Valencia, S.N., Watkins, R.N., and Petro, N.E. (2021) The search for lunar mantle rocks exposed on the surface of the Moon. Nature Communications, 12(1), 1-11.

Moriarty III, D., Watkins, R., Valencia, S., Kendall, J., Evans, A., Dygert, N., and Petro, N. (2021) Evidence for a stratified upper mantle preserved within the South Pole - Aitken Basin. Journal of Geophysical Research: Planets, 126(1), e2020JE006589.

Morris, R., Taylor, G., Newsom, H., Keil, K., and Garcia, S. (1990) Highly evolved and ultramafic lithologies from Apollo 14 soils. Lunar and Planetary Science Conference Proceedings, 20, p. 61-75.

Morrison, D.A. (1998) Did a thick South Pole-Aitken Basin melt sheet differentiate to form cumulates? Lunar and Planetary Science Conference, p. 1657.

Nakamura, R., Matsunaga, T., Ogawa, Y., Yamamoto, S., Hiroi, T., Saiki, K., Hirata, N., Arai, T., Kitazato, K., and Takeda, H. (2009) Ultramafic impact melt sheet beneath the South Pole–Aitken basin on the Moon. Geophysical Research Letters, 36(22).

Nazarov, M., Aranovich, L.Y., Demidova, S., Ntaflos, T., and Brandstätter, F. (2011) Aluminous enstatites of lunar meteorites and deep-seated lunar rocks. Petrology, 19(1), 13-25.

Nazarov, M.A., Demidova, S.I., Patchen, A., and Taylor, L.A. (2004) Dhofar 311, 730 and 731: New lunar meteorites from Oman. Lunar Planet Sci XXXV, 1233.

Nelson, W.S., Hammer, J.E., Shea, T., Hellebrand, E., and Jeffrey Taylor, G. (2021) Chemical heterogeneities reveal early rapid cooling of Apollo Troctolite 76535. Nature Communications, 12(1), 1-9.

Nimis, P., and Taylor, W.R. (2000) Single clinopyroxene thermobarometry for garnet peridotites. Part I. Calibration and testing of a Cr-in-Cpx barometer and an enstatite-in-Cpx thermometer. Contributions to Mineralogy and Petrology, 139(5), 541-554.

Potter, R., Kring, D., Collins, G., Kiefer, W., and McGovern, P. (2012) Estimating transient crater size using the crustal annular bulge: Insights from numerical modeling of lunar basin - scale impacts. Geophysical Research Letters, 39(18).

Powell, R., and Holland, T. (1994) Optimal geothermometry and geobarometry. American Mineralogist, 79(1-2), 120-133.

-. (2008) On thermobarometry. Journal of metamorphic Geology, 26(2), 155-179.

Prissel, T.C., Parman, S., Jackson, C., Rutherford, M., Hess, P., Head, J., Cheek, L., Dhingra, D., and Pieters, C. (2014) Pink Moon: The petrogenesis of pink spinel anorthosites and implications concerning Mg-suite magmatism. Earth and Planetary Science Letters, 403, 144-156.

Prissel, T.C., Parman, S.W., and Head, J.W. (2016) Formation of the lunar highlands Mg-suite as told by spinel. American Mineralogist, 101(7), 1624-1635.

Putirka, K.D. (2008) Thermometers and barometers for volcanic systems. Reviews in Mineralogy and Geochemistry, 69(1), 61-120.

Rapp, J., and Draper, D. (2018) Fractional crystallization of the lunar magma ocean: Updating the dominant paradigm. Meteoritics & Planetary Science, 53(7), 1432-1455.

Saini, R., Mijajlovic, T., Herd, C.D.K., and Walton, E.L. (2022) Northwest Africa 14340: Petrological characterization and shock metamorphism of a lunar regolith breccia. 85th Annual Meeting of The Meteoritical Society, Glasgow, Scotland.

Schmitt, H. (2016) Symplectites in Dunite 72415 and Troctolite 76535 Indicate Mantle Overturn Beneath Lunar Near-Side. 47th Annual Lunar and Planetary Science Conference, p. 2339.

Schwinger, S., and Breuer, D. (2022) Employing magma ocean crystallization models to constrain structure and composition of the lunar interior. Physics of the Earth and Planetary Interiors, 322, 106831.

Shearer, C.K., Burger, P.V., Bell, A.S., Guan, Y., and Neal, C.R. (2015a) Exploring the Moon's surface for remnants of the lunar mantle 1. Dunite xenoliths in mare basalts. A crustal or mantle origin? Meteoritics & Planetary Science, 50(8), 1449-1467.

Shearer, C.K., Elardo, S.M., Petro, N.E., Borg, L.E., and McCubbin, F.M. (2015b) Origin of the lunar highlands Mg-suite: An integrated petrology, geochemistry, chronology, and remote sensing perspective. American Mineralogist, 100(2), 294-325.

Shearer, C.K., and Papike, J. (1999) Magmatic evolution of the Moon. American Mineralogist, 84(10), 1469-1494.

Sheikh, D., Ruzicka, A., Hutson, M.L., and Stream, M. (2022) Dunite clast in lunar meteorites Northwest Africa (NWA) 14900: Mantle Derived? Meteoritics and Planetary Science, 57(S1), 433.

Shervais, J.W., and McGee, J.J. (1999) Petrology of the Western Highland Province: Ancient crust formation at the Apollo 14 site. Journal of Geophysical Research: Planets, 104(E3), 5891-5920.

Shervais, J.W., Taylor, L.A., Laul, J., and Smith, M. (1984) Pristine highland clasts in consortium breccia 14305: Petrology and geochemistry. Journal of Geophysical Research: Solid Earth, 89(S01), C25-C40.

Snyder, G.A., Taylor, L.A., and Halliday, A.N. (1995) Chronology and petrogenesis of the lunar highlands alkali suite: Cumulates from KREEP basalt crystallization. Geochimica et Cosmochimica Acta, 59(6), 1185-1203.

Snyder, G.A., Taylor, L.A., and Neal, C.R. (1992) A chemical model for generating the sources of mare basalts: Combined equilibrium and fractional crystallization of the lunar magmasphere. Geochimica et Cosmochimica Acta, 56(10), 3809-3823.

Spry, A. (1969) Metamorphic Textures. 350 p. Pergamon Press., Oxford, England.

Srivastava, Y., Basu Sarbadhikari, A., Day, J.M., Yamaguchi, A., and Takenouchi, A. (2022) A changing thermal regime revealed from shallow to deep basalt source melting in the Moon. Nature Communications, 13(1), 7594.

Sugihara, T., Ohtake, M., Owada, A., Ishii, T., Otsuki, M., and Takeda, H. (2004) Petrology and reflectance spectroscopy of lunar meteorite Yamato 981031: Implications for the source region of the meteorite and remote-sensing spectroscopy. Antarctic meteorite research, 17, 209.

Taylor, G.J., and Marvin, U.B. (1971) A dunite-norite lunar microbreccia. Meteoritics, 6.

Treiman, A.H., and Coleff, D.M. (2018) Lunar meteorite Northwest Africa (NWA) 11421: X-ray tomography and preliminary petrology. Meteoritics and Planetary Science, 53, Abstract #6329.

Treiman, A.H., Kulis, M.J., and Glazner, A.F. (2019) Spinel-anorthosites on the Moon: Impact melt origins suggested by enthalpy constraints. American Mineralogist: Journal of Earth and Planetary Materials, 104(3), 370-384.

Treiman, A.H., and Semprich, J. (2019) Dunite in lunar meteorite Northwest Africa 11421: Petrology and origin. Lunar and Planetary Science Conference 50th, 50, p. Abstract #1225. Lunar and Planetary Institute, Houston.

Treiman, A.H., and Semprich, J. (2021) Lunar feldspathic breccia Northwest Africa (NWA) 11421: Clasts in the corners. Lunar and Planetary Science Conference 52nd, p. 6065.pdf. Lunar and Planetary Institute Houston TX.

Vaci, Z., Day, J., Paquet, M., Ziegler, K., Yin, Q.-Z., Dey, S., Miller, A., Agee, C., Bartoschewitz, R., and Pack, A. (2021) Olivine-rich achondrites from Vesta and the missing mantle problem. Nature Communications, 12(1), 1-8.

Vaughan, W.M., Head, J.W., Wilson, L., and Hess, P.C. (2013) Geology and petrology of enormous volumes of impact melt on the Moon: A case study of the Orientale basin impact melt sea. Icarus, 223(2), 749-765.

Wager, L., Brown, G., and Wadsworth, W. (1960) Types of igneous cumulates. Journal of Petrology, 1(1), 73-85.

Wager, L.R., and Brown, G.M. (1967) Layered igneous rocks. WH Freeman.

Warren, P.H., Jerde, E.A., and Kallemeyn, G.W. (1987) Pristine Moon rocks: A "large" felsite and a metal - rich ferroan anorthosite. Journal of Geophysical Research: Solid Earth, 92(B4), E303-E313.

Warren, P.H., Taylor, G.J., and Keil, K. (1983) Regolith breccia Allan Hills A81005: Evidence of lunar origin, and petrography of pristine and nonpristine clasts. Geophysical Research Letters, 10(9), 779-782.

Wieczorek, M.A., Jolliff, B.L., Khan, A., Pritchard, M.E., Weiss, B.P., Williams, J.G., Hood, L.L., Righter, K., Neal, C.R., and Shearer, C.K. (2006) The constitution and structure of the lunar interior. Reviews in Mineralogy and Geochemistry, 60(1), 221-364.

Wieczorek, M.A., Neumann, G.A., Nimmo, F., Kiefer, W.S., Taylor, G.J., Melosh, H.J., Phillips, R.J., Solomon, S.C., Andrews-Hanna, J.C., and Asmar, S.W. (2013) The crust of the Moon as seen by GRAIL. Science, 339(6120), 671-675.

Wittmann, A., Korotev, R.L., Jolliff, B.L., and Carpenter, P.K. (2019) Spinel assemblages in lunar meteorites Graves Nunataks 06157 and Dhofar 1528: Implications for impact melting and equilibration in the Moon's upper mantle. Meteoritics & Planetary Science, 54(2), 379-394.

Wood, J.A., Dickey Jr, J.S., Marvin, U.B., and Powell, B.N. (1970) Lunar anorthosites. Science, 167(3918), 602-604.

Yamamoto, S., Nakamura, R., Matsunaga, T., Ogawa, Y., Ishihara, Y., Morota, T., Hirata, N., Ohtake, M., Hiroi, T., and Yokota, Y. (2010) Possible mantle origin of olivine around lunar impact basins detected by SELENE. Nature Geoscience, 3(8), 533-536.

Zeigler, R.A., Coleff, D., and McCubbin, F.M. (2017) The Astromaterials X-Ray Computed Tomography Laboratory at Johnson Space Center. Lunar and Planetary Science Conference.

Zeng, X., Li, S., Joy, K.H., Li, X., Liu, J., Li, Y., Li, R., and Wang, S. (2020) Occurrence and implications of secondary olivine veinlets in lunar highland breccia Northwest Africa 11273. Meteoritics & Planetary Science, 55(1), 36-55.

Zhao, D., Arai, T., Liu, L., and Ohtani, E. (2012) Seismic tomography and geochemical evidence for lunar mantle heterogeneity: Comparing with Earth. Global and Planetary Change, 90, 29-36.

Zhao, Y., De Vries, J., van den Berg, A., Jacobs, M., and van Westrenen, W. (2019) The participation of ilmenite-bearing cumulates in lunar mantle overturn. Earth and Planetary Science Letters, 511, 1-11.

Ziberna, L., Green, E.C., and Blundy, J.D. (2017) Multiple-reaction geobarometry for olivine-bearing igneous rocks. American Mineralogist, 102(12), 2349-2366.